chemosensors

MDPI

Article

Design of A Low-Cost and Disposable Paper-Based Immunosensor for the Rapid and Sensitive Detection of Aflatoxin B1

Fernanda L. Migliorini [1,*,†], Danilo M. dos Santos [1,†], Andrey C. Soares [1], Luiz H. C. Mattoso [1], Osvaldo N. Oliveira, Jr. [2] and Daniel S. Correa [1,*]

1 Nanotechnology National Laboratory for Agriculture, Embrapa Instrumentação, São Carlos 13560-970, SP, Brazil; martinsdanilo.9@gmail.com (D.M.d.S.); andreycoatrini@gmail.com (A.C.S.); luiz.mattoso@embrapa.br (L.H.C.M.)

2 São Carlos Institute of Physics, University of São Paulo, P.O. Box 369, São Carlos 13560-970, SP, Brazil; chu@ifsc.usp.br

* Correspondence: fernandamigliorini@yahoo.com.br (F.L.M.); daniel.correa@embrapa.br (D.S.C.)

† These authors contributed equally to this work.

Received: 7 August 2020; Accepted: 16 September 2020; Published: 20 September 2020

Abstract: We report a paper-based electrochemical immunosensor made with sustainable materials to detect aflatoxin B1 (AFB1), a highly toxic, carcinogenic mycotoxin found in food. The immunosensor was prepared with a waterproof paper substrate and low-cost graphite-based conductive ink through a simple cut-printing method. The working electrode was functionalized with a drop-cast film of multiwalled carbon nanotubes (MWCNT)/chitosan on which a layer of anti-AFB1 monoclonal antibodies was immobilized covalently. The architecture of the immunosensor was confirmed with polarization-modulated infrared reflection absorption spectroscopy (PM-IRRAS) and electrochemical impedance spectroscopy (EIS), including the effective immobilization of the active layer of anti-AFB1. With EIS as the principle of detection, the immunosensor could detect AFB1 in the range from 1 to 30 ng·mL^{-1}, and detection limit of 0.62 ng·mL^{-1}. This sensitivity is sufficient to detect AFB1 in food according to regulatory agencies. The immunosensor exhibited good repeatability, reproducibility, stability, and selectivity in experiments with a possible interferent. Furthermore, detection of AFB1 in maize flour samples yielded recovery of 97–99%, in a demonstration of the possible use of the paper-based immunosensor to detect AFB1 using extraction solutions from food samples.

Keywords: disposable immunosensor; electrochemical detection; aflatoxin B1; chitosan; carbon nanotubes; paper-based sensor

1. Introduction

Aflatoxin B1 (AFB1) is a highly toxic mycotoxin secreted as a secondary metabolite by fungi species such as Aspergillus flavus and Aspergillus parasiticus [1]. It is found as a contaminant in animal feed and agricultural products, particularly in peanuts seeds, wheat, corn, beans, rice, soy, starch, as well as oils and milk [2,3]. Because of its carcinogenic, mutagenic, and teratogenic nature, AFB1 has been associated with deleterious effects on the health of humans and animals [4,5]. It is therefore relevant to develop sensitive, reliable methods for the rapid detection of AFB1. Commonly used analytical methods for AFB1 detection involves enzyme immunoabsorbent assay (ELISA) [6] and chromatographic assays [7] which are time-consuming, costly, and require extensive sample preparation and highly trained personnel [8]. Alternatives to detect trace levels of AFB1 have been electrochemical immunosensors that rely on highly specific antibody-antigen recognition, providing high sensitivity and selectivity, simplicity, low reagent consumption, low detection limit, easy operation, and portability [7,9–11].

Indeed, disposable electrochemical sensors fabricated with low-cost manufacturing processes and sustainable and cheap materials have been used to detect a series of analytes [12–17]. Special attention has been devoted to the preparation of electrodes through printing deposition of single or multiple layers of conductive ink onto a paper substrate [18–22]. Sensors made with conductive graphite-based inks are advantageous owing to the flexibility, low cost, disposability, renewability, and ease of preparation. Their performance can be further improved by modifying the electrodes' surface via deposition of nanoparticles [14,23], conductive polymers [19,24], and carbon-based materials [25,26] because of their stability, electrical conductivity, and large surface area [27,28].

Functionalized multiwalled carbon nanotubes (MWCNTs) have been employed in electrochemical immunosensors [29,30] in order to exploit their electrical properties in addition to their large surface area-to-volume ratios and presence of functional groups for binding antibodies [31–33]. They may be used in conjunction with chitosan, a biopolymer with outstanding characteristics for matrices in biosensors for its biocompatibility, biodegradability, and non-toxicity. Chitosan also possesses reactive functional groups to attach antibodies, including primary amine (-NH_2) and primary and secondary hydroxyl groups (-OH) [34–36]. Therefore, combining carbon nanotubes with chitosan may lead to synergy in reaching a matrix with large number of active sites for immobilization of molecules and enhanced electrochemical properties.

Herein, we developed a disposable paper-based electrochemical immunosensor for the fast and sensitive determination of AFB1 in food samples. The sensing system was fabricated through a simple and low-cost process by using a novel conductive ink composed of shellac, graphite, and carbon black on a waterproof paper substrate. A chitosan/MWCNTs film was then deposited on the working electrode via drop-casting and a layer of antibodies was covalently immobilized. The morphology, spectral characteristics, and electrochemical properties of the immunosensor were investigated. Electrochemical impedance spectroscopy was used for determining the AFB1 concentration. The developed platforms were successfully applied to the rapid, sensitive, and specific determination of AFB1 on extraction solutions from real food samples, thus being promising for food safety monitoring.

2. Experimental Section

2.1. Reagents

Multiwalled carbon nanotubes functionalized with carboxylic acid (MWCNT), aflatoxin B1, anti-AFB1 antibody, ochratoxin A, *N*-ethyl-*N*′-(3-dimethyl aminopropyl) carbodiimide hydrochloride (EDC), *N*-hydroxyl succinimide (NHS), and MES buffer were purchased from Sigma-Aldrich. Chitosan (average degree of deacetylation = 95%; viscosity average molecular weight = 85,000 g·mol^{-1}) was acquired from Cheng Yue Planting Co Ltd (Shenzhen, China) and purified according to the methodology described in ref. [37]. Shellac was purchased from Acrilex (São Bernardo do Campo/SP, Brazil), while graphite and carbon black were acquired from Synth (Diadema/SP; Brazil) and Cabot (Boston, MA, USA), respectively. Adhesive paper was used as substrate from PIMACO (A4 ink-jet/laser 288.5 × 200.0 367 BIC®, Rio de Janeiro/RJ, Brazil).

2.2. Fabrication of Disposable Printed Electrodes

The electrodes were prepared in four stages as illustrated in Figure 1. First, a mixture of graphite/carbon black powders (90/10 (*w*/*w*)) was suspended in shellac in a proportion of 30% (*w*/*w*) and then treated with a disperser type UltraTurrax® (IKA, D125 Basic, Wilmington/NC, USA) for 3 min at 3500 rpm, yielding a homogeneous conductive ink. A thin layer of conductive ink was deposited on the waterproof paper surface by using a paint spatula and dried at 40 °C for 1 h in an air-circulating oven. Masks comprised of working (diameter = 3.3 mm), counter, and reference electrodes were cut from as-prepared conductive sheets by using a cut printer (Silhouette, model 3, Moema/SP, Brazil). The electrodes were removed and glued onto the surface of the waterproof paper,

which was prepared by depositing a layer of shellac onto the paper surface. The electrode was designed with the Silhouette Studio software.

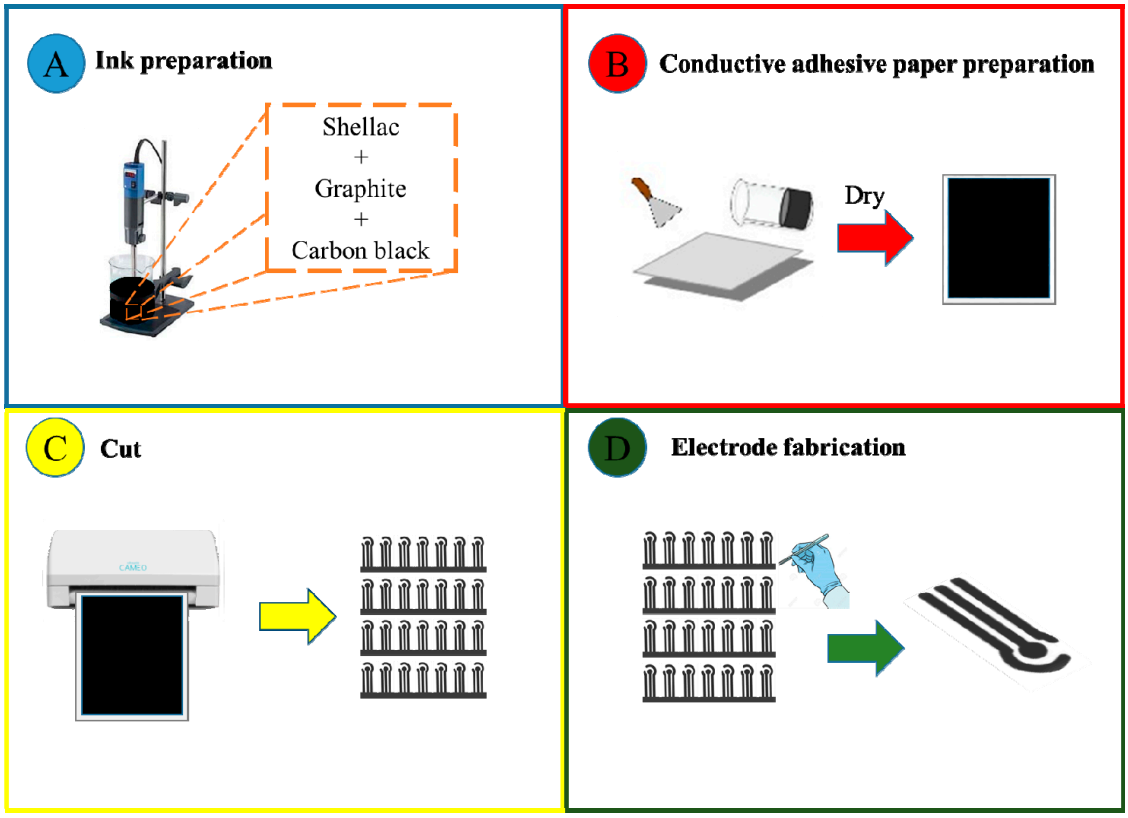

Figure 1. Preparation of disposable electrodes using a simple approach: (**A**) conductive ink preparation; (**B**) application of the conductive ink on a sheet of self-adhesive paper; (**C**) the devices were cut using a silhouette printer; (**D**) next, they were removed and glued onto the surface of the waterproof paper, which was prepared by depositing a layer of shellac onto the adhesive paper surface, being ready for further functionalization.

2.3. Functionalization of Printed Electrodes and Antibody Immobilization

The functionalization of working electrodes was performed using the drop-casting method. MWCNTs were dispersed in a diluted aqueous acetic acid solution (1% (*v*/*v*)) via ultrasound treatment (Branson-Sonifer, model 450D) for 3 min at 20 kHz to result in a concentration of 0.5 mg mL^{-1}. Then, 1 mL of the suspension was mixed with 1 mL of chitosan solution (0.5 mg/mL^{-1}) in the same solvent and placed again in ultrasound treatment under the operational conditions described before. After optimization, 10 µL of filmogenic suspension were deposited onto the working electrode and dried at 30 °C for 40 min in an air-circulating oven. The resulting composite film was neutralized with 10 µL of 1 mol L^{-1} NaOH solution, washed with distilled water, and dried at 30 °C for 40 min. For the immobilization of anti-AFB1, a solution of EDC (0.8 M) and NHS (0.2 M) in 0.1 mol·L^{-1} MES buffer was dripped onto the modified electrode. This solution was maintained in contact with the electrode for 40 min at 25 °C to activate the amine groups from chitosan and the carboxylic groups from MWCNTs [38,39]. After rinsing the electrode with 10 mM PBS (pH 7.4) and drying at room temperature, 10 µL of anti-AFB1 solution (100 µg/mL) in 0.1 mol·L^{-1} MES buffer were deposited onto the modified working electrode and left for 40 min at 25 °C. Next, the electrode was washed with PBS to remove non-immobilized antibodies and dried. In order to block non-active sites [38,40], 10 µL of 5 mg mL^{-1} BSA solution were deposited and let for 30 min at 25 °C. Then, the electrode surface was rinsed with PBS and stored at 4 °C until use.

2.4. Morphological, Structural, and Electrochemical Characterization of Sensing Platforms

The morphology of the nanocomposites was evaluated using field emission scanning electron microscopy (FESEM) with a Philips-XL30 FEG-SEM microscope. Polarized-modulated infrared reflection absorption spectroscopy (PM-IRRAS) (KSV PMI550) was used to investigate the interactions between chitosan/MWCNTs films and anti-AFB1. Electrochemical impedance spectroscopy (EIS) and cyclic voltammetry (CV) measurements were performed using a potentiostat (Autolab PGSTAT 204 Metrohm) controlled with NOVA 2.1 software. The EIS experiments were carried out by applying a voltage of 10 mV AC in the frequency range of 0.1 Hz to 10 kHz with open circuit potential (OCP). The CV tests were performed in the potential range of −0.4 V to 0.4 V using a 5 mM solution of ferri/ferrocyanide $[Fe(CN)_6]^{3-/4-}$ dissolved in 10 mM PBS solution (pH 7.4). A pre-treatment process was performed on the disposable electrodes before the measurements in the potential range of −1.5 V to 1.5 V with a scanning speed of 50 mV using a solution of H_2SO_4 (0.5 mol·L^{-1}).

2.5. Electrochemical Detection of AFB1

A stock solution of AFB1 in methanol (1 μg·mL^{-1}) was prepared and aliquots were diluted with PBS buffer yielding solutions with concentrations from 1 to 30 ng·mL^{-1}, which were used to obtain the calibration curve. In each measurement, 50 μL of AFB1 solution at a given concentration were dropped onto the working electrode and left for 10 min. After rinsing the electrode with PBS, electrochemical impedance measurements were performed in 5 mM of $[Fe(CN)_6]^{3-/4-}$ in PBS. The same electrode was used for measurements of different AFB1 concentrations.

2.6. Data Analysis with Information Visualization Techniques

The Nyquist spectra were processed with the multidimensional projection technique referred to as interactive document mapping (IDMAP) using the Projection Explorer Sensors (Pex-Sensors) software [41,42]. With IDMAP one may obtain 2-D maps by calculating the dissimilarity between two spectra through the Euclidean distance in the original space $X = \{x_1, x_2, \ldots, x_n\}$ and lower dimension space $Y = \{y_1, y_2, ..., y_n\}$. The placement of data points on the 2-D map is made using an error function (injective function) (Equation (1)) that minimizes the term $\left|\delta\left(x_i, x_j\right) - d\left(f\left(x_i\right) - f\left(x_j\right)\right)\right| \forall x_i, x_j \in X$.

$$S_{IDMAP} = \frac{\delta\left(x_i, x_j\right) - \delta_{\min}}{\delta_{\max} - \delta_{\min}} - d\left(y_i, y_j\right) \quad (1)$$

where $\delta_{\max}$ and $\delta_{\min}$ are maximum and minimum distances between data instances, $\delta\left(x_i, x_j\right)$ is the distance between two samples in the original space and $d\left(y_i, y_j\right)$ is the distance between two samples on the projected space (lower dimension space).

2.7. Application of the Immunosensors for Real Food Sample Analysis

Two AFB1-free maize flours from Brazilian brands purchased from a local market were used to prepare solutions with 20 mL methanol/water (80:20, *v*/*v*), 1 g NaCl, and 5 g maize flour. The mixture was shaken for 30 min on the flat mixer and then centrifuged at 6000 rpm for 10 min. An aliquot of 10 mL of the supernatant was diluted with 30 mL PBS and filtered with glass fiber. The extracts were spiked with AFB1 at concentrations varying from 1 to 30 ng mL^{-1} [39].

3. Results and Discussion

3.1. Morphological, Electrochemical, and Spectral Characterization of Electrodes

Field emission scanning electron microscopy (FESEM) was used to evaluate the surface morphology of the working electrodes, and Figure 2A shows a heterogeneous, rough, and lamellar-like surface for the non-modified electrode. The surface of the cast chitosan/MWCNT film deposited onto the working

electrode in Figure 2B is more homogenous and smoother, which was preserved after anti-AFB1 immobilization (Figure 2C).

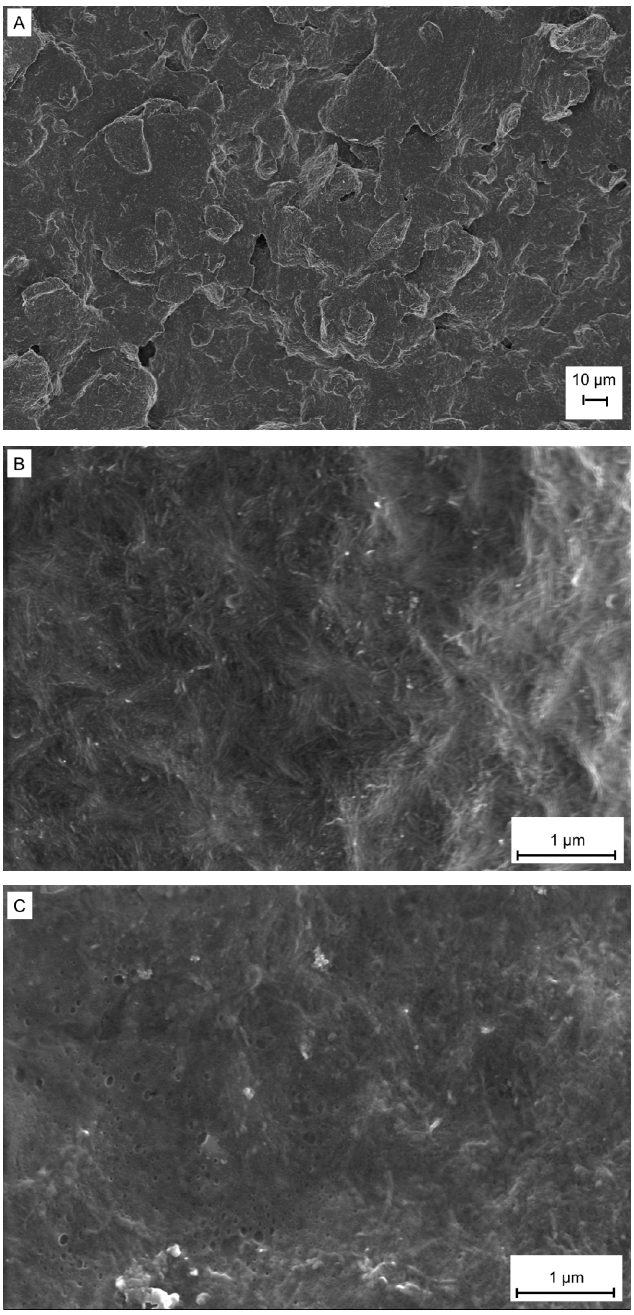

Figure 2. Field emission scanning electron microscopy (FESEM) image of the working electrode before (**A**) and after modification with the chitosan/multiwalled carbon nanotubes (MWCNT) film (**B**) and anti-AFB1 immobilization (**C**).

The electrochemical performance of non-modified electrode upon pretreatment was investigated by using cyclic voltammetry (CV). The potential range was from −1.5 V to 1.5 V in 0.5 mol·L^{-1} H_2SO_4 solution at a scan rate of 50 mV·s^{-1}, and the number of scanning cycles was varied. After each scanning cycle, CV measurements were taken in the presence of the redox probe $Fe(CN)_6]^{3-/4-}$. Figure 3A shows three CV cycles in H_2SO_4, and the CVs in $Fe(CN)_6]^{3-/4-}$ solutions in Figure 3B indicate an increase in the anodic and cathodic current peaks after the pretreatment [43]. This increase is attributed to the activation of the carbon electrode surface. It also demonstrates that pre-treatment with

only one scanning cycle is sufficient to improve the electrode response, which was then adopted in the subsequent electrochemical studies. The electrochemical behavior at different stages of immunosensor preparation was investigated by CV with the redox probe $Fe(CN)_6]^{3-/4-}$, as shown in Figure 3C. The electrodes functionalized with chitosan/MWCNT film had an increased redox peak owing to the MWCNTs. The peak current slightly decreased after antibody immobilization because anti-AFB1 is not conducting. Electrochemical impedance spectroscopy (EIS) also confirmed the increase in conductivity after electrode modification with chitosan/MWCNT film, followed by a decrease with immobilization of anti-AFB1 (Figure 3D). The charge transfer resistance (R_{ct}) for the pristine electrode was 93 Ω, while deposition of the chitosan/MWCNT film changed it to 42 Ω. After immobilization of anti-AFB1, Rct was 86 Ω.

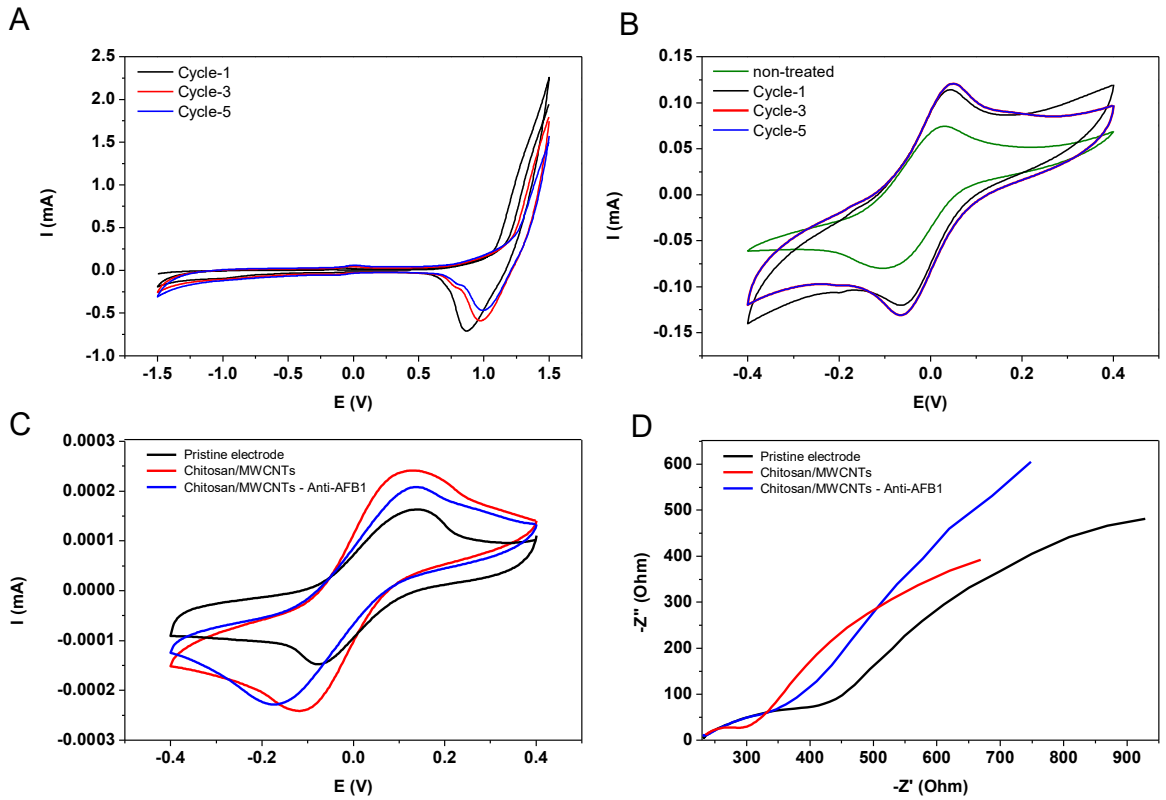

Figure 3. (**A**) Cyclic voltammetry (CV) measurements for 1, 3, and 5 scanning cycles in a solution of H_2SO_4 (0.5 mol L^{-1}) in 50 mV·s^{-1}, for the platform containing graphite, carbon black, and shellac in its composition. (**B**) CV measurements with the redox probe $Fe(CN)_6]^{3-/4-}$ in 10 mM PBS buffer (pH 7.4) with a speed of 100 mV s^{-1} for disposable devices before and after the electrochemical pre-treatment; (**C**) CV and (**D**) electrochemical impedance spectroscopy (EIS) measurements with $Fe(CN)_6]^{3-/4-}$ in 10 mM PBS buffer (pH 7.4) at different stages of immunosensor preparation.

The immobilization of anti-AFB1 on chitosan/MWCNT-modified electrode is also corroborated by comparing the PM-IRRAS spectra in Figure 4. The spectrum of chitosan/MWCNT shows the characteristic bands of chitosan and MWCNT, as follows: The absorption band at 1350 cm^{-1} is due to amide III; the 1570 cm^{-1} band corresponds to the combination of N—H in-plane bending and C—N stretching of amide II; at 1630 cm^{-1} there is C=O stretching of amide I from chitosan [44,45]. The band at 1220 cm^{-1} is attributed to asymmetric stretching of C—O—C and the band at 1740 cm^{-1} is due to C—O carbonyl stretching of MWCNT [33]. Covalent attachment of anti-AFB1 on activated chitosan/MWCNT layer occurs via the linkage between $-NH_2$ groups of chitosan with −COOH groups from anti-AFB1, and through linkage of $-NH_2$ groups of anti-AFB1 with −COOH terminal of MWCNTs resulting in amide bonds [46,47]. As illustrated in Figure 4B, the bands corresponding to amide I and II at 1578 cm^{-1} and 1622 cm^{-1}, respectively, become less intense and are shifted to lower wavenumbers after anti-AFB1

conjugation. These alterations are attributed to the increase in oscillation energy of N-H/C-N dipoles and modification in molecular orientation of N-H/C-N/C=O dipoles [33]. They provide evidence that anti-AFB1 was covalently bound on the activated chitosan/MWCNT layer. In fact, the interaction between AFB1 and the film caused a decrease in band intensity at 1570 and 1630 cm^{-1}. Therefore, the interaction between AFB1 and chitosan/MWCNT film affects the molecular orientation of amide I and II (N-H/C-N/C=O) dipoles from chitosan and AFB1.

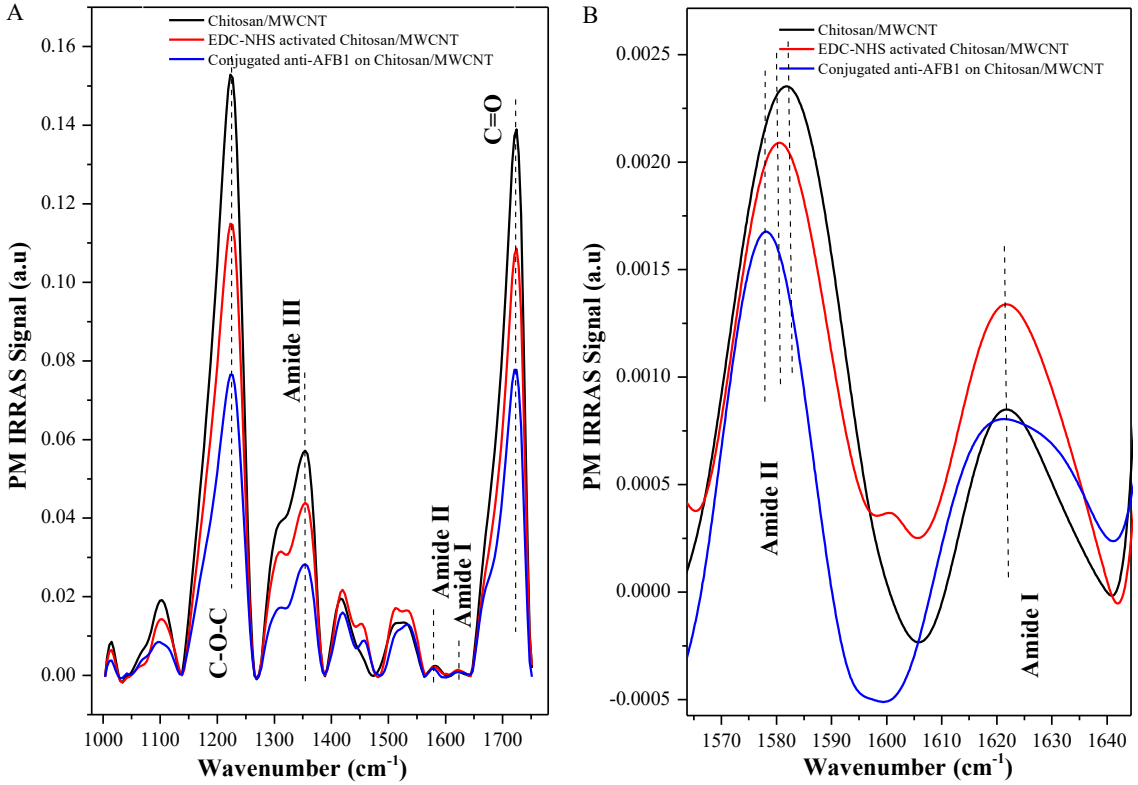

Figure 4. (**A**) Polarization-modulated infrared reflection absorption spectroscopy (PM-IRRAS) spectra for the chitosan/MWCNT at different steps of anti-AFB1 conjugation and (**B**) PM-IRRAS spectra in the range 1565–1645 showing the structural modifications on chitosan/MWCNT layer.

3.2. Electrochemical Detection of Mycotoxin AFB1

The analytical performance of the electrochemical immunosensors to detect AFB1 was evaluated by Faradaic impedance measurements performed with the redox pair ($[Fe(CN)_6]^{3-/4-}$) in triplicate. Figure 5A shows the Nyquist plots for an immunosensor in AFB1 solutions at different concentrations (the whole study included concentrations from 1 to 30 $ng{\cdot}mL^{-1}$, as shown in Figure S1 in the Supplementary Materials). The equivalent circuit used as a model for calculating the values of Rct comprises a resistance associated with the electrolytic solution Rs, and two branches representing the electrolyte-film and the film-substrate interfaces. The branch related to the electrolyte interface contains the double layer capacitance (CdL) and a diffusion impedance defined by a straight line whose inclination is 45° [48], corresponding to the Warburg impedance (represented by a constant phase element CPE)) and a charge transfer resistance (Rct). The branch related to the film-substrate interface comprises a charge transfer resistance (Rct) and the double layer capacitance (CdL). The Rct values decreased linearly with the logarithm of AFB1 concentration, as indicated in Figure 5B. The data can be fitted using linear regression with R_{ct} (Ohm) = −23.08 × log[AFB1] (ng/mL) + 76.93 (R^2 = 0.99). The detection limit (D.L.) of 0.62 $ng{\cdot}mL^{-1}$ was calculated from the ratio between the standard deviation (σ) value of the response of three measurements by using an AFB1 solution with fixed concentration and the slope (S) of calibration curve (D.L. = 3.3 σ/S) [49,50]. This D.L. is below the maximum allowed level

of ABF1 in food established by European Union and the U.S. Food and Drug Administration (FDA) legislation, which are 2 ng·mL^{-1} and 20 ng·mL^{-1}, respectively [51,52]. Hence, this immunosensor is adequate for monitoring food regarding AFB1 contamination.

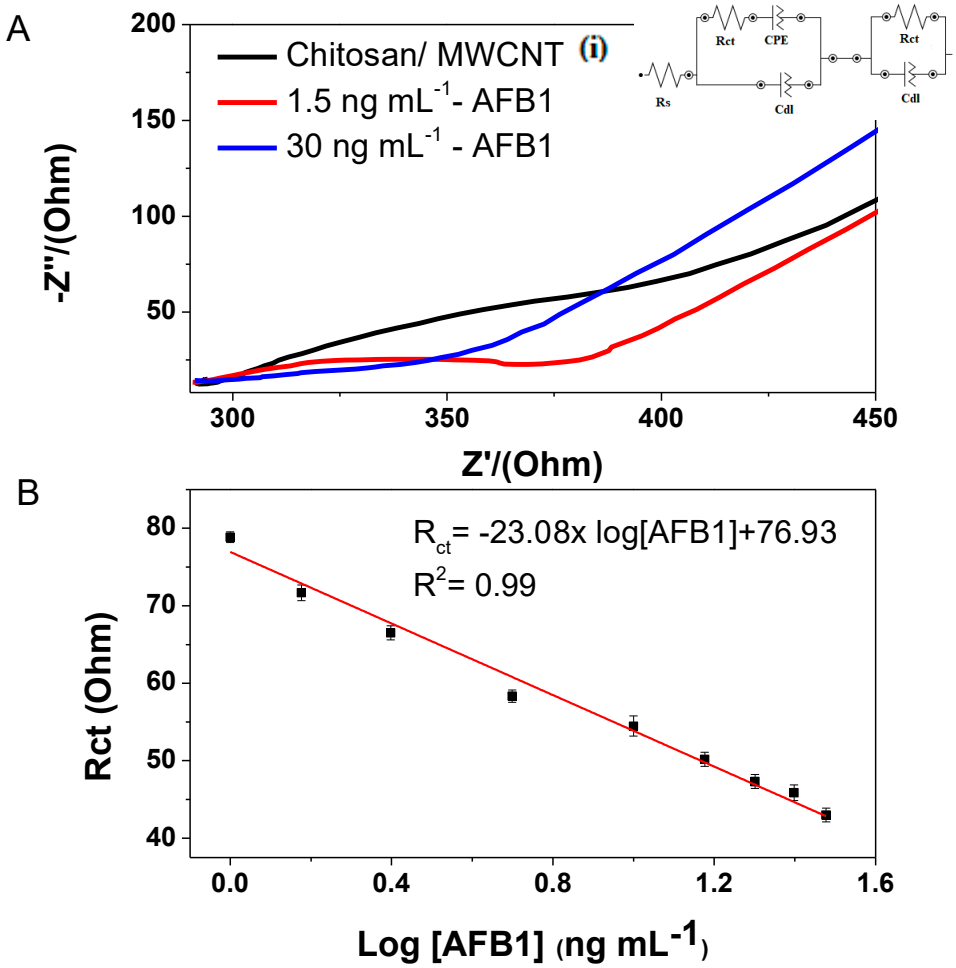

Figure 5. (**A**) Electrochemical impedance measurements for the electrode modified with chitosan/MWCNT films and with the anti-AFB1 immobilized after the antibody/antigen incubation time with different concentrations of AFB1. The inset (i) shows the equivalent circuit model used to fit and analyze the impedance data. (**B**) Rct × logarithm of AFB1 concentration from 1 to 30 ng mL^{-1}.

A visual inspection of the Nyquist plot in Figure 5A,B shows that changes caused by the AFB1-chitosan/MWCNT interaction depend on the AFB1 concentration. This strategy can be complemented by employing information visualization methods. We have used the multidimensional projection interactive document mapping (IDMAP) to generate the 2D plot in Figure 6 using the data of Figure 5A. In the plot, each point represents one Nyquist spectrum for an AFB1 concentration. From Figure 6 one notes a clear separation of the low AFB1 concentrations, up to 10 ng/mL, which is the ideal working concentration range for the immunosensors. At high concentrations the data points tend to cluster together, as expected because in an immunosensor the signal saturates when the majority of adsorption sites are taken.

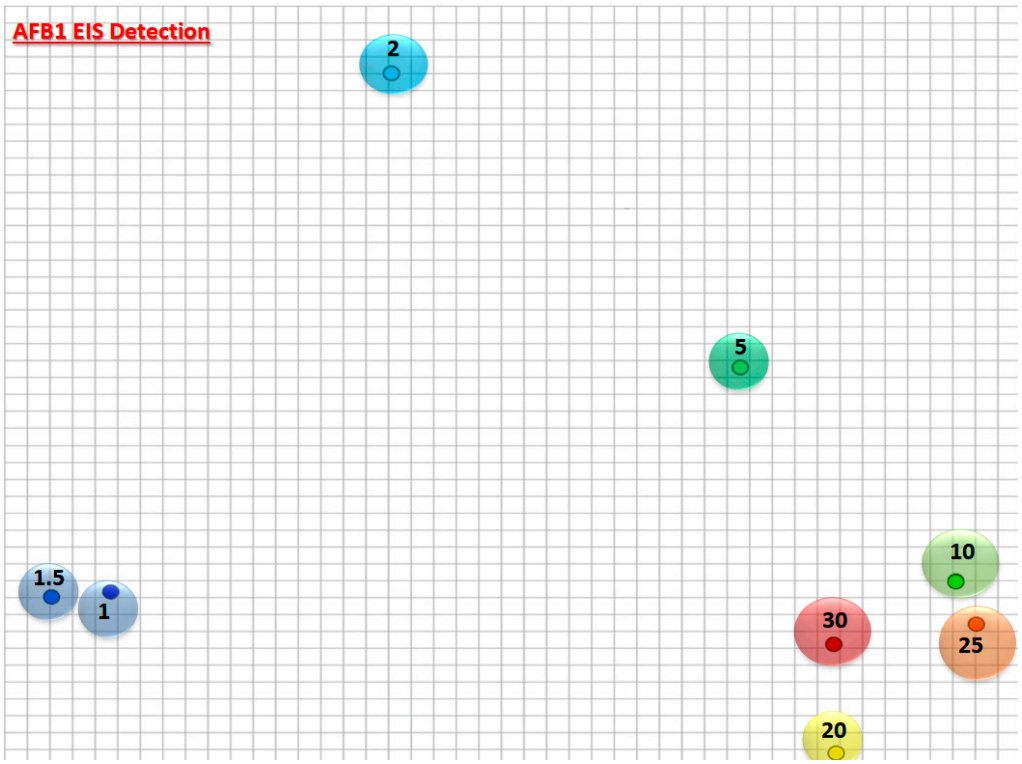

Figure 6. Interactive document mapping (IDMAP) plot obtained from the Nyquist plot of the different AFB1 concentration.

The inter-electrode and intra-electrode reproducibility were verified through repeated experiments using a 20 ng mL^{-1} AFB1 solution. In three successive measurements, the relative standard deviation (RSD) for a given electrode was 3.58%, which increased to 7.80% when three identical electrodes were used. These values indicate that the immunosensors provide reproducible results. The immunosensor stability was assessed by measuring response currents after three weeks of storage at 4 °C. The results revealed that immunosensor maintained 90% of its initial current signal, which indicates its long-term stability for anti-AFB1 detection. The immunosensor had similar performance to others reported in the literature, as shown in Table 1 [39,40,53,54]. As expected, the limit of detection of our immunosensor is not as low as in some of the previous reports, but it is advantageous because the sensing system was fabricated through a simple and low-cost process combined to a novel conductive ink formulation.

Table 1. Comparison of analytical performance of modified electrodes for detection of aflatoxin B1.

Immunoelectrode	Linear Range (ng mL^{-1})	Detection Limit (ng mL^{-1})	Reference
BSA/anti-AFB1/AuNPs	0.001–100	0.0002	53
BSA/anti-AFB1/chitosan-AuNPs	0.1–1; 1–30	0.06	40
BSA/anti-AFB1/chitosan-AuNPs	0.2–2; 2–30	0.12	39
BSA/anti-AFB1/GO	0.05–6	0.05	54
BSA/anti-AFB1/chitosan/MWCNT	1–30	0.62	This work

3.3. Interference Studies and Real Sample Analysis

The selectivity of the electrochemical immunosensors was evaluated in the presence of interfering ochratoxin A, another mycotoxin found in food. Faradaic impedance measurements were performed

with samples containing different concentrations of aflatoxin B1 and ochratoxin A (1 and 30 ng·mL^{-1}) as well as in the presence of both mycotoxins at a concentration of 1 ng mL^{-1} each. Figure 7 shows that R_{ct} did not change in the presence of different concentrations of ochratoxin A. Furthermore, for the measurement using the mixture of the two mycotoxins, the result was similar to the one with aflatoxin B1 only, which demonstrates the high selectivity toward aflatoxin B1.

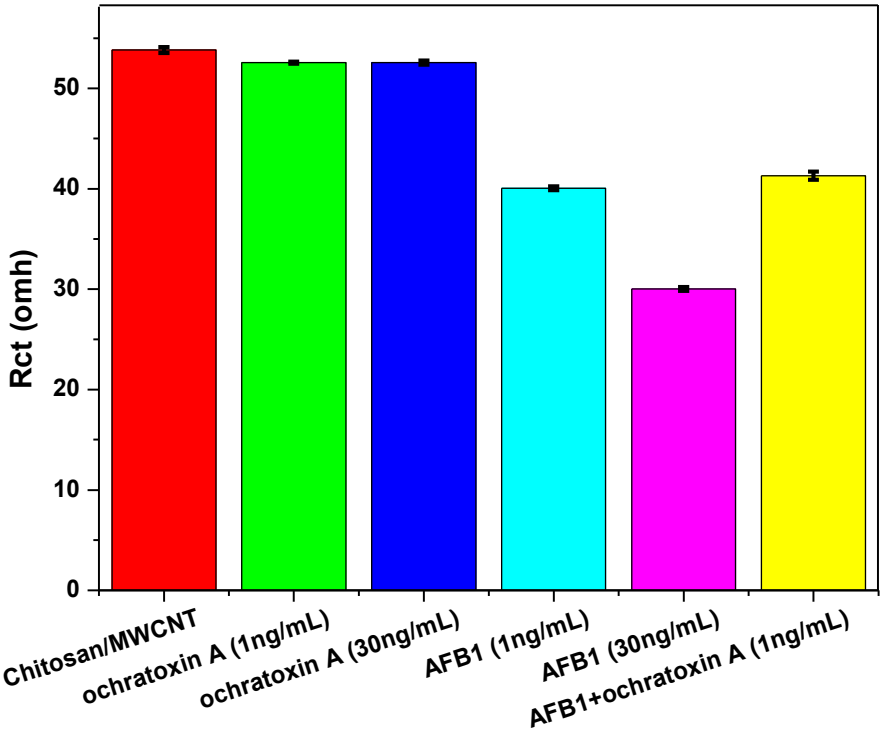

Figure 7. R_{ct} values for the chitosan/MWCNT and chitosan/MWCNT with immobilized anti-AFB1 immunosensor in the presence of interfering mycotoxin (ochratoxin A).

The applicability of the electrochemical immunosensor to detect AFB1 on two brands of commercial maize flour samples was demonstrated. The recovery rates for sample 1 and sample 2 were 97% and 99%, respectively, in a clear evidence of the accuracy and feasibility of the immunosensor to detect AFB1 using extraction solutions from food samples.

4. Conclusions

A low-cost disposable paper-based immunosensor made with chitosan/MWCNT films modified with anti-AFB1 has been employed to detect aflatoxin B1. The impedimetric immunosensor exhibited high sensitivity combined to a suitable detection limit of 0.62 ng mL^{-1} and a linear range of detection from 1 to 30 ng·mL^{-1}. Also, the sensing platform proved useful for detecting aflatoxin B1 using extraction solutions from maize flour samples, and showed high selectivity in the presence of another mycotoxin. This paper-based immunosensor was developed with a simple experimental procedure that can be replicated for other types of biosensors.

Supplementary Materials: The following are available online at http://www.mdpi.com/2227-9040/8/3/87/s1, Figure S1: Electrochemical impedance measurements for the electrode modified with chitosan/MWCNT films and with the anti-AFB1 immobilized after the antibody/antigen incubation time with different concentrations of AFB1 (1 to 30 ng·mL−1).

Author Contributions: F.L.M.: Conceptualization, Writing—original draft, Writing—review and editing, Methodology, Formal analysis. D.M.d.S.: Conceptualization, Writing—original draft, Writing—review and editing, Methodology, Formal analysis. A.C.S.: Writing—review and editing, Methodology, Formal analysis. L.H.C.M.: Supervision, Resources, Writing—review and editing. O.N.O.J.: Supervision, Resources, Writing—review and

editing. D.S.C.: Supervision, Conceptualization, Resources, Writing—review and editing. All authors have read and agreed to the published version of the manuscript.

Funding: This work was financially supported by FAPESP (Grant numbers: 2017/21791-7, 2017/20973-4, 2017/121-74-4, 2018/18953-8, and 2018/22214-6), MCTI-SisNano, CNPq and Rede Agronano (EMBRAPA) from Brazil.

Conflicts of Interest: The authors declare no conflict of interest.

References

1. Xue, Z.; Zhang, Y.; Yu, W.; Zhang, J.; Wang, J.; Wan, F.; Kim, Y.; Liu, Y.; Kou, X. Recent advances in aflatoxin B1 detection based on nanotechnology and nanomaterials-A review. *Anal. Chim. Acta* **2019**, *1069*, 1–27. [CrossRef] [PubMed]
2. Sergeyeva, T.; Yarynka, D.; Piletska, E.; Lynnik, R.; Zaporozhets, O.; Brovko, O.; Piletsky, S.; El'skaya, A. Fluorescent sensor systems based on nanostructured polymeric membranes for selective recognition of Aflatoxin B1. *Talanta* **2017**, *175*, 101–107. [CrossRef] [PubMed]
3. Park, S.; Lee, J.Y.; You, S.; Song, G.; Lim, W. *Neurotoxic Effects of Aflatoxin B1 on Human Astrocytes In Vitro And on Glial Cell Development in Zebrafish In Vivo*; Elsevier B.V.: Amsterdam, The Netherlands; Volume 386, ISBN 8223290499.
4. Wang, C.; Li, Y.; Zhao, Q. A signal-on electrochemical aptasensor for rapid detection of aflatoxin B1 based on competition with complementary DNA. *Biosens. Bioelectron.* **2019**, *144*, 111641. [CrossRef] [PubMed]
5. Rushing, B.R.; Selim, M.I. Aflatoxin B1: A review on metabolism, toxicity, occurrence in food, occupational exposure, and detoxification methods. *Food Chem. Toxicol.* **2019**, *124*, 81–100. [CrossRef]
6. Solanki, P.R.; Singh, J.; Rupavali, B.; Tiwari, S.; Malhotra, B.D. Bismuth oxide nanorods based immunosensor for mycotoxin detection. *Mater. Sci. Eng. C* **2017**, *70*, 564–571. [CrossRef] [PubMed]
7. Uludag, Y.; Esen, E.; Kokturk, G.; Ozer, H.; Muhammad, T.; Olcer, Z.; Basegmez, H.I.O.; Simsek, S.; Barut, S.; Gok, M.Y.; et al. Lab-on-a-chip based biosensor for the real-time detection of aflatoxin. *Talanta* **2016**, *160*, 381–388. [CrossRef]
8. Li, X.; Cao, L.; Zhang, Y.; Yan, P.; Kirk, D.W. Fabrication and Modeling of an Ultrasensitive Label Free Impedimetric Immunosensor for Aflatoxin B1 based on Protein A Self-assembly Modified Gold 3D Nanotube Electrode ensembles. *Electrochim. Acta* **2017**, *247*, 1052–1059. [CrossRef]
9. Myndrul, V.; Viter, R.; Savchuk, M.; Koval, M.; Starodub, N.; Silamiķelis, V.; Smyntyna, V.; Ramanavicius, A.; Iatsunskyi, I. Gold coated porous silicon nanocomposite as a substrate for photoluminescence-based immunosensor suitable for the determination of Aflatoxin B1. *Talanta* **2017**, *175*, 297–304. [CrossRef]
10. Tan, Y.; Wei, X.; Zhang, Y.; Wang, P.; Guo, L.; Lin, Z.; Yang, H. Exonuclease-Catalyzed Target Recycling Amplification and Immobilization Free Electrochemical Aptasensor Exonuclease-Catalyzed Target Recycling Amplification and Immobilization Free Electrochemical Aptasensor. *Anal. Chem.* **2015**. [CrossRef]
11. Sergeyeva, T.; Yarynka, D.; Piletska, E.; Linnik, R.; Zaporozhets, O.; Brovko, O.; Piletsky, S.; El'skaya, A. Development of a smartphone-based biomimetic sensor for aflatoxin B1 detection using molecularly imprinted polymer membranes. *Talanta* **2019**, *201*, 204–210. [CrossRef]
12. Barandun, G.; Soprani, M.; Naficy, S.; Grell, M.; Kasimatis, M.; Chiu, K.L.; Ponzoni, A.; Güder, F. Cellulose Fibers Enable Near-Zero-Cost Electrical Sensing of Water-Soluble Gases. *ACS Sensors* **2019**, *4*, 1662–1669. [CrossRef] [PubMed]
13. Arduini, F.; Cinti, S.; Mazzaracchio, V.; Scognamiglio, V.; Amine, A.; Moscone, D. Carbon black as an outstanding and affordable nanomaterial for electrochemical (bio)sensor design. *Biosens. Bioelectron.* **2020**, *156*, 112033. [CrossRef] [PubMed]
14. Razzino, C.A.; Serafín, V.; Gamella, M.; Pedrero, M.; Montero-Calle, A.; Barderas, R.; Calero, M.; Lobo, A.O.; Yáñez-Sedeño, P.; Campuzano, S.; et al. An electrochemical immunosensor using gold nanoparticles-PAMAM-nanostructured screen-printed carbon electrodes for tau protein determination in plasma and brain tissues from Alzheimer patients. *Biosens. Bioelectron.* **2020**, 112238. [CrossRef] [PubMed]
15. Moro, G.; Bottari, F.; Van Loon, J.; Du Bois, E.; De Wael, K.; Moretto, L.M. Disposable electrodes from waste materials and renewable sources for (bio)electroanalytical applications. *Biosens. Bioelectron.* **2019**, *146*, 111758. [CrossRef] [PubMed]
16. Kurbanoglu, S.; Ozkan, S.A.; Merkoçi, A. Nanomaterials-based enzyme electrochemical biosensors operating through inhibition for biosensing applications. *Biosens. Bioelectron.* **2017**, *89*, 886–898. [CrossRef]

17. de Oliveira, T.R.; Fonseca, W.T.; de Oliveira Setti, G.; Faria, R.C. Fast and flexible strategy to produce electrochemical paper-based analytical devices using a craft cutter printer to create wax barrier and screen-printed electrodes. *Talanta* **2019**, *195*, 480–489. [CrossRef]
18. Zhu, G.; Yin, X.; Jin, D.; Zhang, B.; Gu, Y.; An, Y. Paper-based immunosensors: Current trends in the types and applied detection techniques. *TrAC Trends Anal. Chem.* **2019**, *111*, 100–117. [CrossRef]
19. Huang, X.; Shi, W.; Li, J.; Bao, N.; Yu, C.; Gu, H. Determination of salivary uric acid by using poly(3,4-ethylenedioxythipohene) and graphene oxide in a disposable paper-based analytical device. *Anal. Chim. Acta* **2020**, *1103*, 75–83. [CrossRef]
20. Cincotto, F.H.; Fava, E.L.; Moraes, F.C.; Fatibello-Filho, O.; Faria, R.C. A new disposable microfluidic electrochemical paper-based device for the simultaneous determination of clinical biomarkers. *Talanta* **2019**, *195*, 62–68. [CrossRef]
21. Orzari, L.O.; Cristina de Freitas, R.; Aparecida de Araujo Andreotti, I.; Gatti, A.; Janegitz, B.C. A novel disposable self-adhesive inked paper device for electrochemical sensing of dopamine and serotonin neurotransmitters and biosensing of glucose. *Biosens. Bioelectron.* **2019**, *138*, 111310. [CrossRef]
22. Orzari, L.O.; de Araujo Andreotti, I.A.; Bergamini, M.F.; Marcolino, L.H.; Janegitz, B.C. Disposable electrode obtained by pencil drawing on corrugated fiberboard substrate. *Sensors Actuators B Chem.* **2018**, *264*, 20–26. [CrossRef]
23. Agrisuelas, J.; González-Sánchez, M.I.; Valero, E. Hydrogen peroxide sensor based on in situ grown Pt nanoparticles from waste screen-printed electrodes. *Sensors Actuators B Chem.* **2017**, *249*, 499–505. [CrossRef]
24. Qin, Q.; Bai, X.; Hua, Z. Electropolymerization of a conductive β-cyclodextrin polymer on reduced graphene oxide modified screen-printed electrode for simultaneous determination of ascorbic acid, dopamine and uric acid. *J. Electroanal. Chem.* **2016**, *782*, 50–58. [CrossRef]
25. Kampeera, J.; Pasakon, P.; Karuwan, C.; Arunrut, N.; Sappat, A.; Sirithammajak, S.; Dechokiattawan, N.; Sumranwanich, T.; Chaivisuthangkura, P.; Ounjai, P.; et al. Point-of-care rapid detection of Vibrio parahaemolyticus in seafood using loop-mediated isothermal amplification and graphene-based screen-printed electrochemical sensor. *Biosens. Bioelectron.* **2019**, *132*, 271–278. [CrossRef] [PubMed]
26. Dias, A.A.; Cardoso, T.M.G.; Chagas, C.L.S.; Oliveira, V.X.G.; Munoz, R.A.A.; Henry, C.S.; Santana, M.H.P.; Paixão, T.R.L.C.; Coltro, W.K.T. Detection of Analgesics and Sedation Drugs in Whiskey Using Electrochemical Paper-based Analytical Devices. *Electroanalysis* **2018**, *30*, 2250–2257. [CrossRef]
27. Hernández-Ibáñez, N.; García-Cruz, L.; Montiel, V.; Foster, C.W.; Banks, C.E.; Iniesta, J. Electrochemical lactate biosensor based upon chitosan/carbon nanotubes modified screen-printed graphite electrodes for the determination of lactate in embryonic cell cultures. *Biosens. Bioelectron.* **2016**, *77*, 1168–1174. [CrossRef]
28. Ochiai, L.M.; Agustini, D.; Figueiredo-Filho, L.C.S.; Banks, C.E.; Marcolino-Junior, L.H.; Bergamini, M.F. Electroanalytical thread-device for estriol determination using screen-printed carbon electrodes modified with carbon nanotubes. *Sensors Actuators B Chem.* **2017**, *241*, 978–984. [CrossRef]
29. Serafín, V.; Valverde, A.; Martínez-García, G.; Martínez-Periñán, E.; Comba, F.; Garranzo-Asensio, M.; Barderas, R.; Yáñez-Sedeño, P.; Campuzano, S.; Pingarrón, J.M. Graphene quantum dots-functionalized multi-walled carbon nanotubes as nanocarriers in electrochemical immunosensing. Determination of IL-13 receptor A2 in colorectal cells and tumor tissues with different metastatic potential. *Sensors Actuators B Chem.* **2019**, *284*, 711–722. [CrossRef]
30. Ganbat, K.; Pan, D.; Chen, K.; Ning, Z.; Xing, L.; Zhang, Y.; Shen, Y. One-pot electrografting preparation of bifunctionalized carbon nanotubes for sensitive electrochemical immunosensing. *J. Electroanal. Chem.* **2020**, *860*, 113906. [CrossRef]
31. Atashbar, M.Z.; Bejcek, B.; Singamaneni, S.; Santucci, S. Carbon nanotube based biosensors. *Proc. IEEE Sens.* **2004**, *2*, 1048–1051. [CrossRef]
32. Gupta, S.; Murthy, C.N.; Prabha, C.R. Recent advances in carbon nanotube based electrochemical biosensors. *Int. J. Biol. Macromol.* **2018**, *108*, 687–703. [CrossRef] [PubMed]
33. Thapa, A.; Soares, A.C.; Soares, J.C.; Awan, I.T.; Volpati, D.; Melendez, M.E.; Fregnani, J.H.T.G.; Carvalho, A.L.; Oliveira, O.N. Carbon Nanotube Matrix for Highly Sensitive Biosensors to Detect Pancreatic Cancer Biomarker CA19-9. *ACS Appl. Mater. Interfaces* **2017**, *9*, 25878–25886. [CrossRef]
34. Negm, N.A.; Hefni, H.H.H.; Abd-Elaal, A.A.A.; Badr, E.A.; Abou Kana, M.T.H. Advancement on modification of chitosan biopolymer and its potential applications. *Int. J. Biol. Macromol.* **2020**, *152*, 681–702. [CrossRef] [PubMed]

35. Liu, X.; Sakthivel, R.; Liu, W.C.; Huang, C.W.; Li, J.; Xu, C.; Wu, Y.; Song, L.; He, W.; Chung, R.J. Ultra-highly sensitive organophosphorus biosensor based on chitosan/tin disulfide and British housefly acetylcholinesterase. *Food Chem.* **2020**, *324*, 126889. [CrossRef]
36. Kaur, N.; Bharti, A.; Batra, S.; Rana, S.; Rana, S.; Bhalla, A.; Prabhakar, N. An electrochemical aptasensor based on graphene doped chitosan nanocomposites for determination of Ochratoxin A. *Microchem. J.* **2019**, *144*, 102–109. [CrossRef]
37. dos Santos, D.M.; Bukzem, A.D.L.; Campana-Filho, S.P. Response surface methodology applied to the study of the microwave-assisted synthesis of quaternized chitosan. *Carbohydr. Polym.* **2016**, *138*, 317–326. [CrossRef]
38. Yu, L.; Zhang, Y.; Hu, C.; Wu, H.; Yang, Y.; Huang, C.; Jia, N. Highly sensitive electrochemical impedance spectroscopy immunosensor for the detection of AFB 1 in olive oil. *FOOD Chem.* **2015**, *176*, 22–26. [CrossRef]
39. Ma, H.; Sun, J.; Zhang, Y.; Xia, S. Disposable amperometric immunosensor for simple and sensitive determination of aflatoxin B1 in wheat. *Biochem. Eng. J.* **2016**, *115*, 38–46. [CrossRef]
40. Ma, H.; Sun, J.; Zhang, Y.; Bian, C.; Xia, S.; Zhen, T. Label-free immunosensor based on one-step electrodeposition of chitosan-gold nanoparticles biocompatible film on Au microelectrode for determination of aflatoxin B1 in maize. *Biosens. Bioelectron.* **2016**, *80*, 222–229. [CrossRef]
41. Paulovich, F.V.; Moraes, M.L.; Maki, R.M.; Ferreira, M.; Oliveira, O.N.; de Oliveira, M.C.F. Information visualization techniques for sensing and biosensing. *Analyst* **2011**, *136*, 1344–1350. [CrossRef]
42. Minghim, R.; Paulovich, F.V.; de Andrade Lopes, A. Content-based text mapping using multi-dimensional projections for exploration of document collections. *Vis. Data Anal.* **2006**, *6060*, 60600S. [CrossRef]
43. Bernalte, E.; Marín-Sánchez, C.; Pinilla-Gil, E.; Brett, C.M.A. Characterisation of screen-printed gold and gold nanoparticle-modified carbon sensors by electrochemical impedance spectroscopy. *J. Electroanal. Chem.* **2013**, *709*, 70–76. [CrossRef]
44. Lawrie, G.; Keen, I.; Drew, B.; Chandler-Temple, A.; Rintoul, L.; Fredericks, P.; Grøndahl, L. Interactions between alginate and chitosan biopolymers characterized using FTIR and XPS. *Biomacromolecules* **2007**, *8*, 2533–2541. [CrossRef] [PubMed]
45. Mallamace, F.; Corsaro, C.; Mallamace, D.; Vasi, S.; Vasi, C.; Dugo, G. The role of water in protein's behavior: The two dynamical crossovers studied by NMR and FTIR techniques. *Comput. Struct. Biotechnol. J.* **2015**, *13*, 33–37. [CrossRef]
46. Gao, Y.; Kyratzis, I. Covalent Immobilization of Proteins on Carbon Nanotubes Using the. *Bioconjug. Chem.* **2008**, *19*, 1945–1950. [CrossRef]
47. Jin, W.J.; Yang, G.J.; Shao, H.X.; Qin, A.J. A novel label-free impedimetric immunosensor for detection of semicarbazide residue based on gold nanoparticles-functional chitosan composite membrane. *Sensors Actuators B Chem.* **2013**, *188*, 271–279. [CrossRef]
48. Almeida, D.A.L.; Edwards, E.R.; Ferreira, N.G. Self-sustaining hybrid electrode prepared from polyaniline, carbon nanotubes, and carbon fibers: Morphological, structural, and electrochemical analyses. *J. Solid State Electrochem.* **2018**, *22*, 69–80. [CrossRef]
49. Comité de Direcção ICH Validation of Analytical Procedures: Text and Methodology Q2(R1). *Int. Conf. Harmon.* **2005**, *1994*, 17.
50. Currie, L.A. International Union of Pure and Applied Chemistry Nomenclature in Evaluation of Analytical Methods Including Detection and Quantification Capabilities. *Pure Appl. Chem.* **1995**, *67*, 1699–1723. [CrossRef]
51. Ren, M.; Xu, H.; Huang, X.; Kuang, M.; Xiong, Y.; Xu, H.; Xu, Y.; Chen, H.; Wang, A. Immunochromatographic assay for ultrasensitive detection of aflatoxin B1 in maize by highly luminescent quantum dot beads. *ACS Appl. Mater. Interfaces* **2014**, *6*, 14215–14222. [CrossRef]
52. Krittayavathananon, A.; Sawangphruk, M. Impedimetric Sensor of ss-HSDNA/Reduced Graphene Oxide Aerogel Electrode toward Aflatoxin B1 Detection: Effects of Redox Mediator Charges and Hydrodynamic Diffusion. *Anal. Chem.* **2017**, *89*, 13283–13289. [CrossRef] [PubMed]

53. Wang, H.; Zhang, Y.; Chu, Y.; Ma, H.; Li, Y.; Wu, D.; Du, B.; Wei, Q. Disposable competitive-type immunoassay for determination of aflatoxin B1 via detection of copper ions released from Cu-apatite. *Talanta* **2016**, *147*, 556–560. [CrossRef] [PubMed]
54. Goud, K.Y.; Hayat, A.; Catanante, G.; Satyanarayana, S.M.; Gobi, K.V.; Marty, J.L. An electrochemical aptasensor based on functionalized graphene oxide assisted electrocatalytic signal amplification of methylene blue for aflatoxin B1 detection. *Electrochim. Acta* **2017**, *244*, 96–103. [CrossRef]